PALACKY UNIVERSITY OLOMOUC
FACULTY OF NATURAL SCIENCES

Department of Optics

Polarization state control using liquid crystals

BACHELOR THESIS

Vojtěch Krčmarský

2014

PALACKY UNIVERSITY OLOMOUC
FACULTY OF NATURAL SCIENCES

Department of Optics

Polarization state control using liquid crystals

BACHELOR THESIS

Author:	Vojtěch Krčmarský
Study programme:	B1701 Physics
Field of study:	Optics and optoelectronics
Form of study:	Full - time
Supervisor:	Mgr. Miroslav Ježek, Ph.D.
Co-supervisor:	Mgr. Michal Mičuda, Ph.D.

UNIVERZITA PALACKÉHO V OLOMOUCI
PŘÍRODOVĚDECKÁ FAKULTA

Katedra optiky

Využití kapalných krystalů pro ovládání polarizačního stavu světla

BAKALÁŘSKÁ PRÁCE

Vypracoval:	Vojtěch Krčmarský
Studijní program:	B1701 Fyzika
Studijní obor:	Optika a optoelektronika
Forma studia:	prezenční
Vedoucí bakalářské práce:	Mgr. Miroslav Ježek, Ph.D.
Konzultant bakalářské práce:	Mgr. Michal Mičuda, Ph.D.

Abstract

Liquid crystals find a wide range of use in optical experiments where they can replace elements such as quarter wave plates or half wave plates. Their main advantages are fast change of polarization state and small dimensions. The main goal of this experimentally oriented Thesis is to test properties of liquid crystal modules to effectively control the polarization state of light.

Keywords

polarization, liquid crystals, liquid crystal display, segment display, pixel display

Acknowledgement

I would like to thank my supervisor Mgr. Miroslav Ježek, Ph.D. for his advices, guidance, consultations and patience. My thanks belong to my co-supervisor Mgr. Michal Mičuda, Ph.D for his consultations and advices. I am grateful to other members of Department of Optics, especially Mgr. Martina Miková and Mgr. Ivo Straka, for creating supportive and friendly environment. I would also like to thank my family for their support, patience and love. Last but not least, I would like to thank my roommate Pavel Zoufalý for cheering up. Special thanks go to OCZ Vrchlabí company.

Declaration

I declare that I have written Bachelor Thesis "Polarization state control using liquid crystals"on my own under the guidance of Mgr. Miroslav Ježek, Ph.D. by using theoretical resources, which are referred to in the list of literature. I agree with the further usage of this document according to the requirements of the Department of Optics.

In Olomouc on .....

Contents

1 Introduction

Liquid crystals were first observed by Austrian botanist Friedrich Reinitzer in 1888 [1]. Since then liquid crystal technology developed rapidly. Their main use is in display technology. Nowadays we can find these materials in almost every device from digital watches, pocket calculators, mobile phones to large television screens [2]. The basic property of liquid crystals is the ability to change the polarization state of incoming light.

Liquid crystal technology can also be used for scientific purposes. For example, it can be used for construction of a tunable narrow band frequency Lyot filter [3]. It can be used for polarimeters, where they could replace a rotating quarter wave plate. We would like to use this technology in quantum information processing with linear optics and single photons, where quantum bits are encoded into polarization state of light. Almost every operation on polarization of light needs at least one fixed wave plate and if we want to prepare the polarization state and reconstruct it we need two pairs of rotatable wave plates. These optical elements with rotation stages take a lot of space and the process of state preparation could take tens of seconds. Liquid crystal devices can change the polarization state of light in time interval of tenths of seconds simply by applying proper voltage and dimensions of such devices are in order of millimeters. We can also use liquid crystal modules for modulating of the polarization state of close interfering beams. This application requires high quality of wavefront and phase stability.

There are several manufacturers involved in making such devices for scientific purposes. Their devices meet high standards for optical measurements, but the price is adequately high. There are also groups of scientists who made their own liquid crystal modules. For example, K. Hirabayashi presented the liquid crystal device that is able to simulate the action of rotatable quarter wave plate or half wave plate but only aperture surface of 40 μm^2[4]. Other scientists have developed various instruments using liquid crystals. J. M. Bueno presented experimental setup that uses liquid crystal modules for measuring elements of Mueller matrices of various optical elements [5]. Z. Zhuang, S.-W. Suh, and J. S. Patel described the construction of a polarization state controller using three liquid crystal modules [6].

The main goal of this Thesis is to become familiar with liquid crystal technology, examine the behavior of various liquid crystal devices and test the possibility of using common liquid crystal displays in experiments performed in Quantum Optics Laboratory

Olomouc. If it turns out that some of tested technology is suitable for our purposes, it could replace the quarter wave plates or half wave plates in some experiments. These devices could also allow us to control polarization states of two or more close parallel beams independently.

This Thesis consists of three main parts. The first part includes basic information about the liquid crystal technology and basic mathematical background for describing the action of liquid crystals on the polarization state of light and the description of a method used for the polarization state analysis. The second part describes a setup used for measurements and liquid crystal devices that were put under test. The third part discusses measurements and their results.

2 Theory

2.1 Principle of liquid crystal display technology

Liquid crystal is fluid phase of matter where molecules have the orientation order like crystals but their spatial order is similar to liquids. There are many categories of liquid crystals. We can divide them into two main classes: lyotropic and thermotropic [1, 7]. Lyotropic group exhibits liquid crystal behavior when it reacts with a specific solvent. We can find these materials in biological structures such as cell walls or brain cells [1]. Second group of liquid crystals are thermotropic liquid crystals. They are changing state from liquid crystals to isotropic fluid while the temperature grows and this process is generally reversible [1]. The thermotropic group can be further divided by the shape of molecules to cigar-like and disc-like [1]. Liquid crystals used in LC displays are almost always cigar-like.

We recognize three phases or types of thermotropic liquid crystal - smectic, nematic and cholesteric [1, 7, 8]. For smectic liquid crystals it is typical that molecules of liquid crystal are organized in series of layers [1, 8]. The long axis of the cigar-like molecules are parallel one to each other and are perpendicular to the layer plane [1]. Nematic liquid crystals form a "thread-like structure"[1]. The order of molecules in this state is not as high as in smectic phase, but they maintain the parallel orientation. Nematic liquid crystals are usually oriented in one direction which is given by a vector $\vec{n}$ called director. This molecular alignment causes anisotropic characteristics, the physical properties such as refractive index, electrical conductivity, permeability, etc. are different for the direction of the long axis and the direction of plane normal to the long axis [1]. For example, the refractive index along the director $\vec{n}$ is usually larger than in perpendicular direction, permeability is generally negative and its absolute value is smaller along the director axes than in perpendicular direction [1]. These crystals are usually used in liquid crystal displays. The third phase of liquid crystals is called cholesteric because of presence of a large number of compounds containing cholesterol [1]. These molecules are also arranged in layers and similarly to the nematic liquid crystals molecules are aligned parallel. The difference between cholesteric and nematic phase is that molecules in cholesteric phase lie in thin layers whose directors are not parallel to each other. The orientation displacement causes that the cholesteric liquid crystals follow a helical structure [1]. This specific structure causes selective reflection in wavelength and also causes circular polarization [7]. They are used as additives in TN and STN displays [1]. The phases of liquid crystals are schematically shown in Fig. 1.

Liquid crystal displays use the birefringence property of liquid crystals which causes the

change of the polarization state of incident light. These materials possess both linear and circular anisotropy at the same time [9]. Liquid crystals are easily oriented or deformed by electric field, magnetic field, heat or mechanical stress. These outer forces can change the birefringence property of liquid crystals [1, 7].

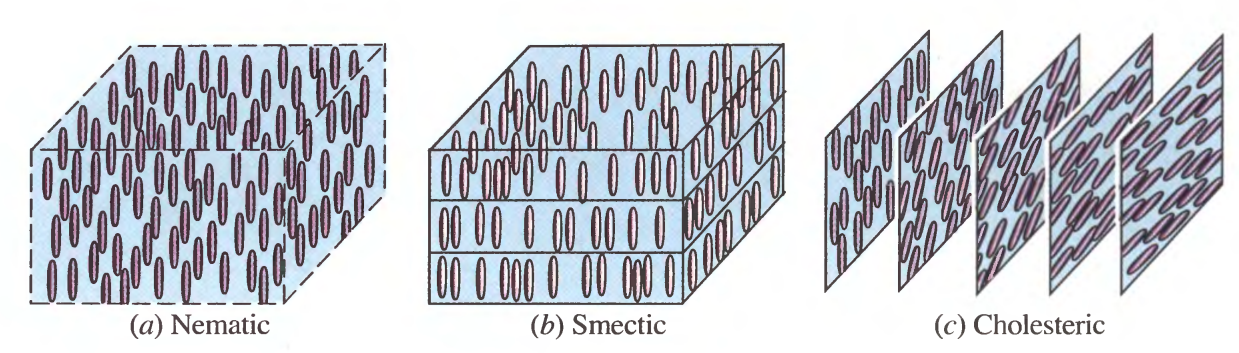

Figure 1: Molecular alignment of different types of liquid crystals: (a) nematic; (b) smectic; (c) cholesteric [8].

2.2 Structure and driving of LC displays

The basic structure of all liquid crystal displays is pictured in Fig. 2. Unpolarized light gets polarized by the first polarizer and passes through an active area with liquid crystals. The thickness of this part is usually in order of tens of micrometers. The polarization state of the light changes by liquid crystals. On the other side of the device, there is another glass plate and the second polarizer. Depending on the polarization before the second polarizer the light passes through this polarizer or it is stopped. The configuration of polarizers orientation depends on the technology used. Inner sides of the glass plates are covered with two layers: the Indium Tine Oxide (ITO) layer and the alignment layer. The ITO layer works as electrode and it is also responsible for the shape of controllable segments of the display. ITO is transparent conductive material that consists of about 90% of In_2O_3 and 10% SnO_2 [10]. Applying voltage to the ITO layer modifies the orientation of liquid crystals in the device. The alignment layer is responsible for overall alignment of liquid crystals. Materials used for this layer, usually polyimides, are thermally stable, easy to apply to surface and cheap [11]. The layer itself does not make crystals oriented the way we need. It is necessary to create a structure of microscopic grooves, that allow crystals to align. Molecules of liquid crystal fill these grooves and rest of them will orient themselves parallel, see Fig. 3. There exist several methods to achieve that. The oldest, but still

used method is called rubbing. The polymer surface is rubbed with a velvet cloth in one direction so needed structure is created [11]. The resulting layer is very stable. The main disadvantage of this method is debris left on the alignment layer after the rubbing process [11]. Another disadvantage of this process is the possible creation of electrostatic charge that can destroy electronic part of the display and can result for example in dead pixel [11]. Different technique, that can create such structure, is photoalignment. This technology uses the interaction of polyimides with linearly polarized deep UV light [12]. If the electric field direction of the incident polarized UV light agrees with the molecules transition moment, the molecule strongly absorbs the light causing a photochemical reaction [12, 13]. This method eliminates most problems of rubbing technique, among them the electrostatic charges and rests of the material after rubbing [11, 13]. This technology is suitable for curved and flexible substrates [13].

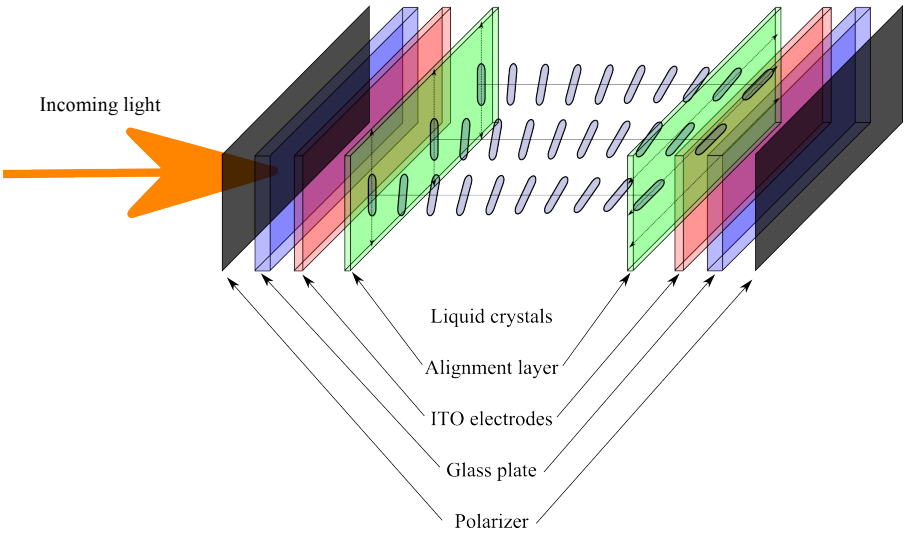

Figure 2: Structure of common liquid crystal device. Configuration of liquid crystal molecules without applied voltage.

A voltage applied to display electrodes causes redirection of molecules of liquid crystal, see Fig. 4. If the applied voltage is high enough, the molecules of the liquid crystal orient in a way that the propagating light is not affected by birefringence property of the liquid crystal and the polarization state does not change. The driving voltage must be a square wave signal without DC component. If applied voltage has the DC component, the population of free ions inside the liquid crystal layer grows and induces strong fields around alignment layers [14]. It causes chemical changes of liquid crystals, and ultimately, their destruction. A growing number of free ions is due to selective adsorption of alignment

Figure 3: Molecules of LC filling grooves in alignment layer [1].

layers [14, 15]. All voltages mentioned in this Thesis are therefore amplitudes of the square wave.

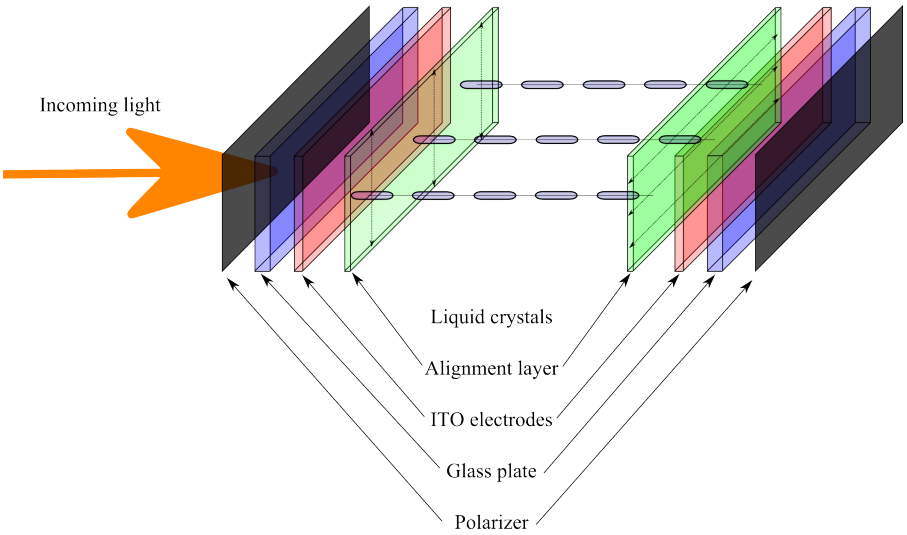

Figure 4: Liquid crystal module with applied voltage. Liquid crystal molecules are oriented in direction of the voltage. Light is not affected by birefringence of LCs.

2.3 TN and STN technology

TN stands for Twisted Nematic. The TN technology uses nematic liquid crystals to guide light propagating across the module. The twist of crystal is similar to twist that cholesteric liquid crystals create but is invoked by property of nematic liquid crystal that its molecules tend to orient themselves parallel to substrate between which they are filled (see section

2.2). If we orient the front and the rear glass plate in a way that the alignment layers are crossed, we create a helical structure with 90 degrees twist.

In STN (Super Twisted Nematic) modules the liquid crystals inside the cell twist more than 90 degrees and less than 360 degrees. The typical value of the twist, for this kind of displays, is 270 degrees. Another property that differs regular TN and STN is the deviation of director orientation from perpendicular to the orientation of the alignment layer. This is achieved by doping the nematic liquid crystals with cholesteric type [1]. Higher twist angle causes steeper dependence of light transmission on applied voltage. That causes that the "on"and "off"states are closer and helps to achieve higher contrast [2]. This difference is depicted in Fig. 5.

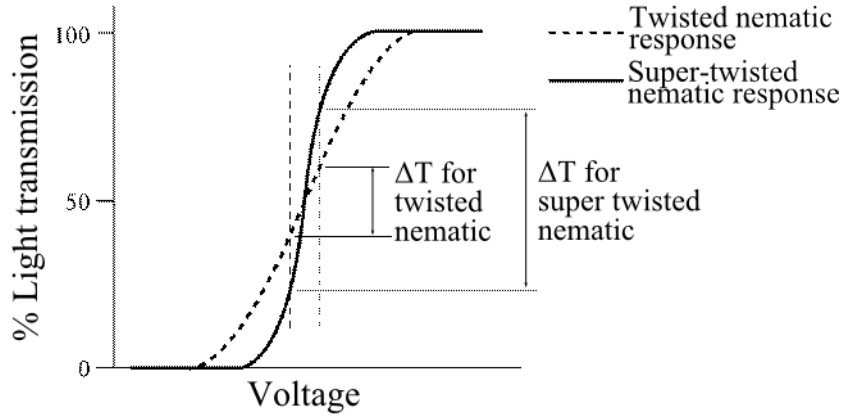

Figure 5: Comparison of dependence of light transmission on applied voltage for TN and STN technology [16].

2.4 Theoretical model

Every polarization state can be represented, in analogy with the two level mixed quantum system, by a density matrix

$$\rho = \sum_k p_k \left|k\right\rangle \left\langle k\right|, \tag{1}$$

where p_k is the probability of finding the pure state $|k\rangle$ in the given mixtureρ. This states can also be described by 4 dimensional Stokes vector

$$S = \begin{bmatrix} S_0 \\ S_1 \\ S_2 \\ S_3 \end{bmatrix} = \begin{bmatrix} 1 \\ r\cos(2\theta)\cos(2\nu) \\ r\sin(2\theta)\cos(2\nu) \\ r\sin(2\nu) \end{bmatrix}. \tag{2}$$

Parameter S_0 is equivalent to total intensity and is set to 1 for normalization purposes and r is equivalent to the degree of polarization (DOP) given by

$$DOP = \sqrt{S_1^2 + S_2^2 + S_3^2} = r. \tag{3}$$

Because both density matrix and Stokes vector describe the polarization state equivalently, we can find relation between them and get the density matrix from Stokes vector using

$$\rho = \frac{1}{2}\left[\sigma_0 + \sum_{i=1}^{3}(S_i\sigma_i)\right], \tag{4}$$

where S_i are Stokes parameters and σ_i is one of Pauli matrices:

$$\sigma_0 = \begin{pmatrix} 1 & 0 \\ 0 & 1 \end{pmatrix},\ \sigma_1 = \begin{pmatrix} 1 & 0 \\ 0 & -1 \end{pmatrix},\ \sigma_2 = \begin{pmatrix} 0 & 1 \\ 1 & 0 \end{pmatrix},\ \sigma_3 = \begin{pmatrix} 0 & -i \\ i & 0 \end{pmatrix}. \tag{5}$$

The pure states ($DOP = 1$) can be described by the 2 dimensional Jones vector

$$|\psi\rangle = \begin{bmatrix} \cos\theta \\ \sin\theta\exp(i\nu) \end{bmatrix}. \tag{6}$$

In both Jones and Stokes formalisms the angles θ and ν represent longitude and latitude on Poincaré sphere. This is graphically represented in Fig. 6. The purity of polarization state is given by $\mathrm{Tr}\,[\rho^2]$ and is equal to $\frac{1}{2}(1 + DOP^2)$. In my measurements I have worked with 6 main polarization states which are represented by following Stokes vectors:

$$|H\rangle = \begin{bmatrix} 1 \\ 1 \\ 0 \\ 0 \end{bmatrix}, |V\rangle = \begin{bmatrix} 1 \\ -1 \\ 0 \\ 0 \end{bmatrix}, |D\rangle = \begin{bmatrix} 1 \\ 0 \\ 1 \\ 0 \end{bmatrix}, |A\rangle = \begin{bmatrix} 1 \\ 0 \\ -1 \\ 0 \end{bmatrix}, |R\rangle = \begin{bmatrix} 1 \\ 0 \\ 0 \\ 1 \end{bmatrix}, |L\rangle = \begin{bmatrix} 1 \\ 0 \\ 0 \\ -1 \end{bmatrix}. \tag{7}$$

Here $|H\rangle$ means horizontal state, $|V\rangle$ vertical, $|D\rangle$ diagonal, $|A\rangle$ antidiagonal, $|R\rangle$ right hand circular and $|L\rangle$ left hand circular polarization state. In this Thesis I also use notation H, V, D, A, R or L respectively for these states. Table 1 shows angles 2θ and 2ν on Poincaré sphere in range $[0; 2\pi)$ for this 6 main states.

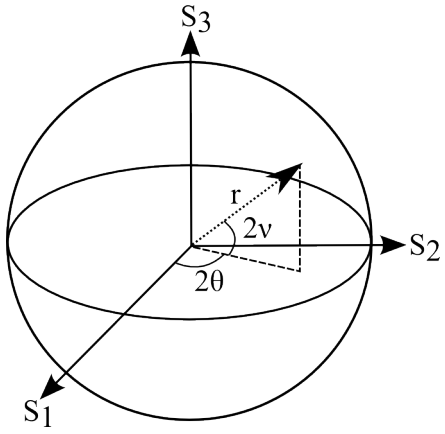

Figure 6: Poincaré sphere....

	H	V	D	A	R	L
2θ	0	$\pi;\ 0$	$\frac{\pi}{2}$	$\frac{3\pi}{2};\ \frac{\pi}{2}$	NA	NA
2ν	0	$0;\ \pi$	0	$0;\ \pi$	$\frac{\pi}{2}$	$\frac{3\pi}{2}$

Table 1: Angles 2θ and 2ν.

Optical elements are then described by matrices with dimension 2×2 in Jones formalism and 4×4 in Stokes-Mueller formalism. For pure states both formalisms are equivalent and so there is a transition between Jones matrices and Mueller matrices given by [17]:

$$M_{ij} = \frac{1}{2}\,\mathrm{Tr}\left[J\sigma_j J^{\dagger}\sigma_i\right], \tag{8}$$

where M_{ij} is ij element of 4×4 Mueller matrix, J is the corresponding Jones matrix, $\dagger$ represents Hermitian conjugation and σ_i is one of Pauli matrices (5). Using this formula we can determine the Mueller matrix for liquid crystal devices, where we use following Jones matrix [9]

$$J_{LC} = \begin{pmatrix} \cos\chi - i\left(\frac{\delta}{\chi}\right)\sin\chi & \left(\frac{\varphi}{\chi}\right)\sin\chi \\ -\left(\frac{\varphi}{\chi}\right)\sin\chi & \cos\chi + i\left(\frac{\delta}{\chi}\right)\sin\chi \end{pmatrix}. \tag{9}$$

In this matrix $\chi^2 = \varphi^2 + \delta^2$. φ represents twist angle while retardation δ represents difference of refraction index along slow and fast axis. From (9) it is obvious that liquid crystals can exhibit properties of both linear and circular birefringence at the same time [9, 19]. Using formula (8) we can find elements of Mueller matrix of LC module. The

matrix is then given by

$$M_{\mathrm{LC}} = \begin{bmatrix} 1 & 0 & 0 & 0 \\ 0 & \left(\frac{\delta}{\chi}\right)^2 + \left(\frac{\varphi}{\chi}\right)^2 \cos 2\chi & \frac{\varphi}{\chi}\sin 2\chi & -2\left(\frac{\delta\varphi}{\chi^2}\right)\sin^2\chi \\ 0 & -\frac{\varphi}{\chi}\sin 2\chi & \cos 2\chi & -\frac{\delta}{\chi}\sin 2\chi \\ 0 & -2\left(\frac{\delta\varphi}{\chi^2}\right)\sin^2\chi & \frac{\delta}{\chi}\sin 2\chi & \left(\frac{\varphi}{\chi}\right)^2 + \left(\frac{\delta}{\chi}\right)^2 \cos 2\chi \end{bmatrix}, \tag{10}$$

which is unitary transformation because $M_{\mathrm{LC}}^{\dagger} \cdot M_{\mathrm{LC}} = \sigma_0$ and $|\det M_{\mathrm{LC}}| = 1$.

The birefringence and therefore retardation δ changes with applied voltage. The measured dependence of δ on the voltage is given in various documents, such as data sheets from manufacturers of the devices (e.g. [18]). To describe the dependence I have developed a theoretical model based on logistic distribution curve described as

$$\delta(V) = \frac{a}{b + e^{d - c \cdot V^e}} + f, \tag{11}$$

where *a, b, c, d, e* and *f* are parameters and V is variable voltage. Some authors work with arctan function instead [20]. For fitting purposes I have rewrote this function

$$\delta(V) = d + a \arctan\left(bV + c\right), \tag{12}$$

where a, b, c and d are parameters and V is the voltage.

To predict trajectory of polarization state on Poincaré sphere with varying voltage, we can use standard Mueller-Stokes calculus. The theoretical output state is given by equation

$$S_{\mathrm{OUT}} = R(\xi) \cdot M_{\mathrm{LC}} \cdot R(-\xi) \cdot S_{\mathrm{IN}}, \tag{13}$$

where S_{IN} is Stokes vector of input state. The rotation matrix with arbitrary angle ξ is used because the orientation of liquid crystals with respect to used measurement basis was unknown.

2.5 Polarization analysis and state reconstruction

The direct reconstruction of the polarization state of the light is used to determine the polarization state after propagating through the liquid crystal module. This method is based on projecting an unknown state to three independent bases H/V, D/A and R/L. For example, if we look for a probability p_H of state H we measure intensities of projections to H and V. The probability of finding H state in the measured state is given by $p_H = \frac{I_H}{I_H + I_V}$, where I_H and I_V are measured intensities. Other probabilities are calculated analogously, explicitly:

$$\langle H|\rho|H\rangle = p_H = \frac{I_H}{I_H + I_V}, \tag{14a}$$

$$\langle D|\rho|D\rangle = p_D = \frac{I_D}{I_D + I_D}, \tag{14b}$$

$$\langle R|\rho|R\rangle = p_R = \frac{I_R}{I_R + I_R}. \tag{14c}$$

In these equations ρ is the density matrix (4). By solving equations (14a-c) we get formulas for calculating the Stokes parameters from measured intensities:

$$S_1 = \frac{2I_H}{I_H + I_V} - 1, \tag{15a}$$

$$S_2 = \frac{2I_D}{I_D + I_A} - 1, \tag{15b}$$

$$S_3 = \frac{2I_R}{I_R + I_L} - 1. \tag{15c}$$

To probe an unknown operation of a liquid crystal module, I repeat this state reconstruction procedure at the output of the module for six main polarization states at the input. The whole measurement can be performed for various voltages applied to the liquid crystal module. For each output state all six intensities are measured. To find values of the parameters that occur in theoretical calculations, namely parameters of the models (11) and (12), rotation ξ, and twist φ I have numerically solved the least squares problem given by the expression

$$\sum_{\mathrm{l=H,V,D,A,R,L}} \sum_{m=1}^{3} \sum_{n=1}^{N} \left[(S_{l,m,n} - T_{l,m,n})^2 \right], \tag{16}$$

where $S_{l,m,n}$ is the $\mathrm{m^{th}}$ component of measured Stokes vector with applied voltage corresponding to $\mathrm{n^{th}}$ measurement with input polarization H, V, D, A, R and L, and $T_{l,m,n}$ is theoretical model for each $S_{l,m,n}$. As the result we obtain the parameters values fitting all the input states at the same time.

Statistical uncertainties were determined from measured values of photocurrent as uncertainty type A. Uncertainties of Stokes parameters S_1, S_2 and S_3 as well as the uncertainty of the DOP were calculated using the law of error propagation.

3 Experiments

3.1 Setup

The majority of measurements presented in this Thesis are based on probing an LC module by various polarization states and analysis by means of full state tomography described in section 2.5. The experimental setup consists of four main parts and its scheme is depicted in Fig.7. Photo of real experiment is shown in Fig. 8.

I have used the QPhotonics laser diode QFLD-810-10S with central wavelength 800 nm. The signal is then led through a single mode optical fiber (Nufern 780 HP [21]) to a collimator (Schäfter+Kirchhoff 60FC-4-A11-02, SN: 000702) where the light is decoupled from the optical fiber to free space. Second part of the setup prepares an initial polarization state. The laser beam goes through a polarizer P1 (Thorlabs LP VIS100) fixed in horizontal direction. The beam then enters a sequence of wave plates where the arbitrary polarization state can be prepared. In my experiment, I have used a configuration where the beam goes first through a quarter-wave plate (QWP1) and then through half wave plate (HWP1).

In the third part of the setup there is a device under test. In this case a liquid crystal module is situated here. To this part we can count electronics that drives the LC module (e.g. signal generator or Arduino board). On the LC module there is also a platinum temperature probe connected to the Hameg 8112-3 multimeter to measure the temperature of the LC module.

The last section of the setup is polarization state analysis and detection. It consists of sequence of wave plates and polarizer, similarly to the polarization state generation in part one of the setup, but with opposite order. There is the half wave plate (HWP2), followed by a quarter wave plate (QWP2) and polarizer (P2) fixed in vertical direction. All wave plates used in this setup are designed for wavelength of 800 nm and supplied by Altechna company and are mounted in motorized stages Newport SR50CC and controlled by SMC100CC controller. Finally, there is a photodiode Thorlabs DET36A, that detects the intensity of incident light and transforms it into a photocurrent, which is measured using the TTi 1906 multimeter.

The whole experiment is controlled through a computer, which runs my Python program. This software controls rotations of all 4 wave plates, voltage that drives the LC module, and reading data from multimeters. Multimeters and motorized stages are connected to the computer via RS232 interface, while the signal generator is connected via USB.

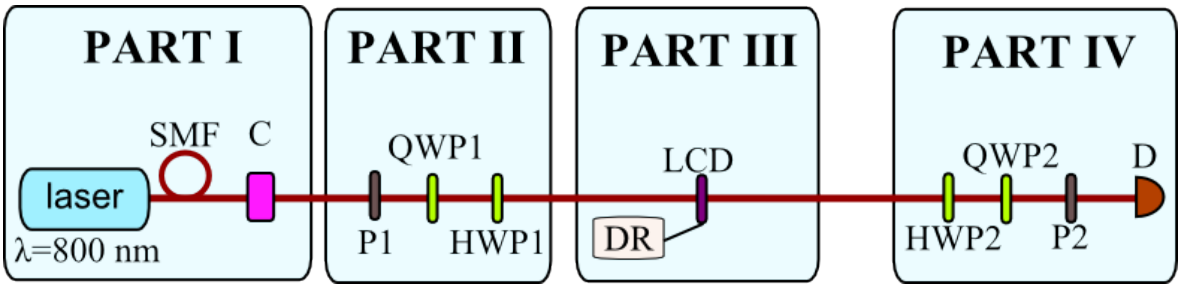

Figure 7: Scheme of the experiment. The light from laser diode goes through a single mode optical fiber (SMF) to a collimator C, where is decoupled to free space. The light then passes through a polarization state preparation (PART II) consisting of polarizer P1 set to H and wave plates QWP1 and HWP1. Then the light passes through the LCD module, driven by electronics DR (PART III) and after that goes through state analysis (PART IV), that consists of waveplates HWP2, QWP2 and polarizer P2. The light is then detected by photodiode D.

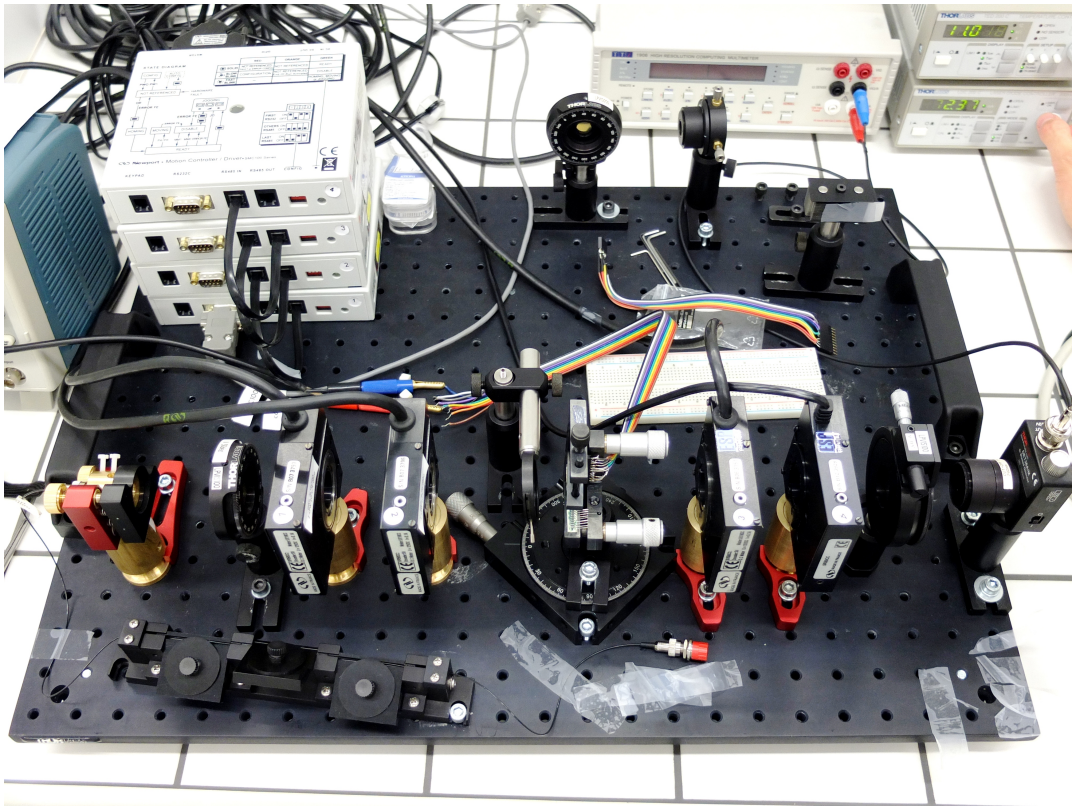

Figure 8: Photo of thel experiment setup.

3.2 Segment displays

Segment displays are commonly used in electronic devices, such as digital watches or calculators. Displays are filled with liquid crystals and the shapes of segments are created using various techniques. We can find displays with many different shapes of segments. For our purposes, it is very important that the segments are large enough for the laser beam. The electrodes usually have a direct pin connection.

For driving the segment LC displays I have used the Tektronix AFG3252 (see [22] for datasheet) function generator. This instrument allows us to create a square wave with zero DC component and amplitude up to 5 V. We can also connect this device to a computer via USB using USBTMC protocol. For communication with a PC we also need a communication library called Virtual Instrument Software Architecture (VISA). Tektronix, the manufacturer of the generator, provides on its website a free version of this software called TekVISA. Using this and the pyVISA library for Python it is very simple to control the device using PC. The voltage signal is applied to display pins connected directly to the display electrodes, which are responsible for orientation of liquid crystals in each segment.

I have tested two types of segment displays. First I have worked with RS 5080PHR 215-6442, the scheme of which is shown in Fig. 9. This figure shows also a connection of pins to electrodes of each segment. I have used segment 1C for measurements.

Second display from segment display group was OCZ 2027. This display is made by TN270° technology. The scheme of the display with described segments is shown in figure 10. This display has the alignment layer oriented in 45° (diagonal). In my experiments I have used segment 18.

All displays were used with all polarization, protective and reflective layers removed and the surface was cleaned from any rests of glue using isopropanol or aceton. Segment displays without any layers are called segment modules in this Thesis.

3.3 Pixel displays

Nowadays, pixel displays are very often used in almost every device. Using pixel display we can create every shape that we want, using square segments called pixels (picture elements) that are filling the whole area of the display. To make pixel displays easy to drive, manufacturers usually use control chips, that addresses each pixel separately. The communication with the display is then established using defined communication protocol.

The parameter that describes number of these pixels in the display is the resolution. Another important parameter that is even more significant for our purpose is fill factor. It

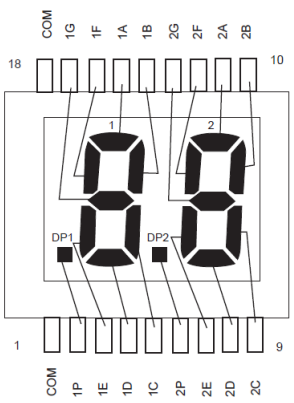

Figure 9: Layout of RS 5080PHR 215-6442 display with the scheme of pins connection [23]. Segment 1C was examined in experiments.

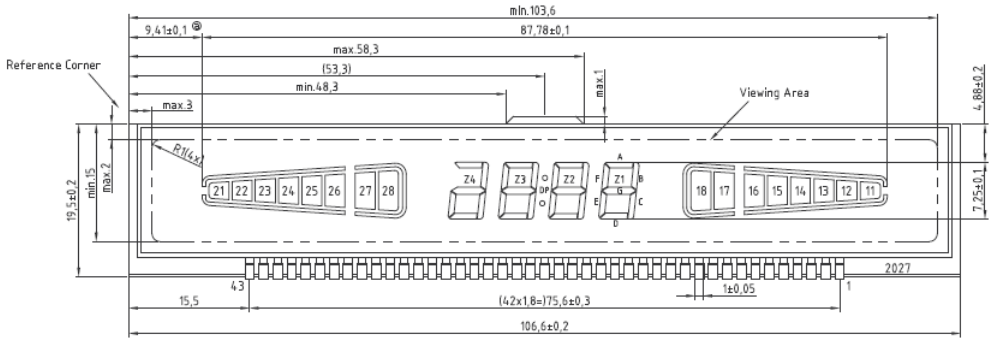

Figure 10: Layout of the OCZ 2027. Segment 18 was used in my experiments.

shows how much of area of the display is actually active and controllable in respect to the whole area of the display. This factor is given by

$$FF = \frac{S_{\mathrm{PIX}}}{S_{\mathrm{A}}}, \tag{17}$$

where S_{PIX} is total area of all pixels in the display and S_{A} is total area of the display filled with liquid crystals.

I have tested displays from Electronic Assembly's DOG XL160 family. These displays have 160 pixels in each row and 104 pixels in each column and use the STN technology. Dimensions of the pixel in these displays are 0.397 mm × 0.418 mm and dimensions of the whole area with liquid crystal is 69.265 mm × 42.833 mm. That gives fill factor for DOG XL160 $FF = 0.93$. The scheme of the display with the dimensions of pixels and gaps between them is depicted in Fig. 11.

Parameter	Number of levels	Affects
Gray level	4	each pixel
Contrast	256	all pixels

Table 2: Parameters of *DOG XL* displays that can be set externally.

The DOG XL displays are controlled by 3.3 V signal logic and the pixels of the display are addressed by a control chip UC 1610. The communication with the chip can be provided by four types of serial modes. The 2-wire I^2C mode, 3-wire 8 bit SPI mode, 4-wire 8 bit SPI mode and 3-wire 9 bit SPI mode. I have chosen the 4-wire 8 bit SPI mode for communication with the chip. For driving this displays I have used the Arduino UNO board based on ATMEL 8-bit ATmega328 microcontroller. Unfortunately, Arduino UNO uses a 5 V logic signal so I had to use the logic converter CMOS type 74HC4050E. The Arduino board was programmed through a computer using Arduino software. The layout of the connection is in Fig. 13.

The UC1610 chip can control various properties. The most important for us is the ability to set the "gray level"of each pixel, which is equivalent to applying voltage to segments of a segment display. Unfortunately the UC1610 chip provides only 4 possible values of the "gray level ". This is very limiting for our use. Second property that we can change is "contrast"of the display. This option affects all pixels in the display. The parameters of DOG XL160 displays, that we can control, are shown in Tab. 2. I have made a program to drive this display via Arduino board based on the DOGM128 library [24].

Another display of this kind that I have worked with was OCZ 2001. This display uses a STN180° technology. As we can see from the scheme in Fig. 12, the display has a segment part and a pixel part, but only the pixel part was used. This particular display was prepared as a sample by OCZ Vrchlabí company for testing purposes. It shares properties of the pixel and segment displays. The display has a matrix of pixels, but does not have any control chip and also we cannot control each pixel separately, we can only drive whole column of 9 pixels connected together to one pin where the driving voltage signal is applied. Dimensions of this display are 43.1 mm $\times$ 24.2mm but the size of the pixel area is only 17.89 mm $\times$ 6.98 mm and every pixel has size 0.731×0.731 mm. Tha gap between pixels is 0.05 mm. This gives us a fill factor $FF \approx 0.88$.

All pixel displays were used without any polarization, protection or reflective layers and were cleaned from any rests of glue the same way as segment ones. Pixel displays without

any layers are called pixel modules in this Thesis.

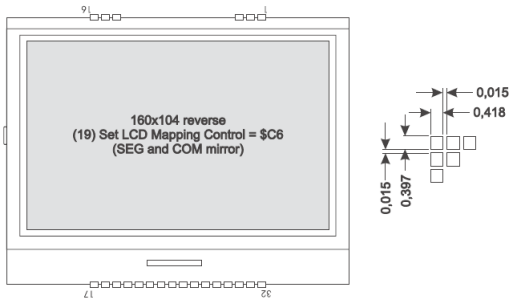

Figure 11: Layout of the *DOG XL* display with dimensions of pixels and gaps [25].

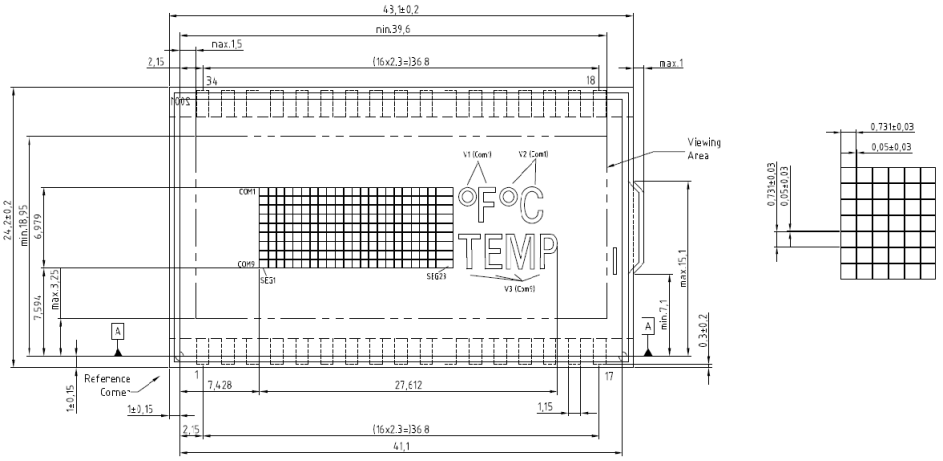

Figure 12: Layout of the *OCZ 2001* display with dimensions of the module, pixels and gaps between pixels.

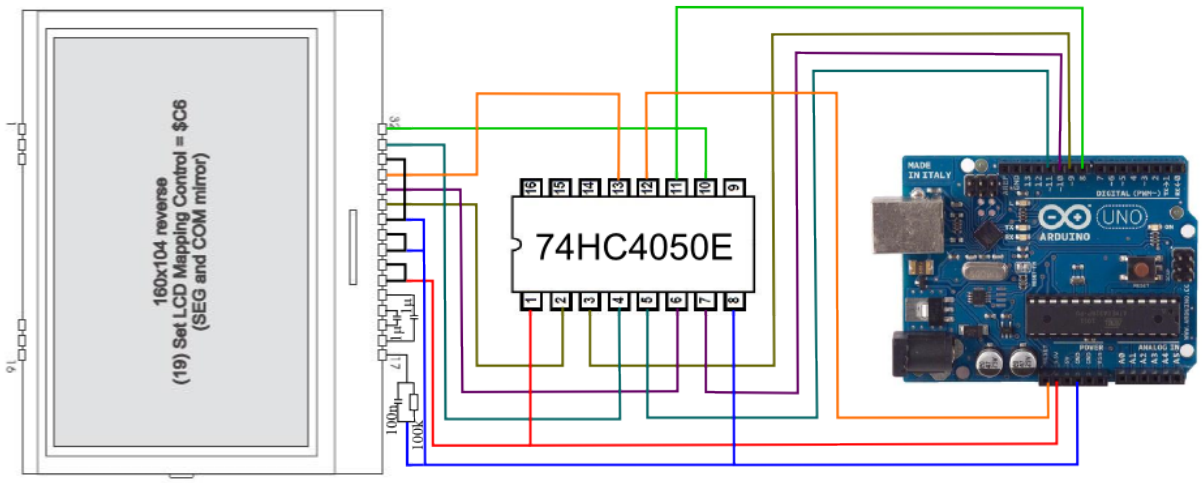

Figure 13: Scheme of the circuit with Arduino Uno board, CMOS convertor and DOG display. Signal generated by Arduino board in 5 V logic is transformed by the CMOS 74HC4050E chip to 3.3 V logic and then the signal is applied to the pins of display.

4 Measurements and results

The primary point of my interest was to look at the transformation of polarization state by a LC module. I was changing applied voltage and measured the output polarization state and degree of polarization. The Stokes vectors were calculated as described in Section 2.5. I have likewise done a temperature stability measurement to determine the influence of temperature on liquid crystals and to assess effects of the liquid crystals on the stability of the whole experimental setup.

4.1 Segment module *RS 5080PHR 215-6442*

Effect on polarization state

The polarized light was weakly focused by collimator the C, see Fig. 7, on the segment 1C of this module, see Fig. 9. The polarization state was then transformed by the liquid crystal. Figures 15 and 16 show the transformation of polarization state dependent on the applied voltage for 6 input states (H, V, D, A, R and L). Graphs on the left side of each figure show Stokes parameters (S_1, S_2 and S_3) of the output state depending on applied voltage and on the right side of each figure there is a Poincaré sphere where the measured states are fitted with a theoretical curve. Table 3 shows achieved minimum and maximum output degree of polarization for all input states. I have also calculated value of redardance δ. This dependence is in the graph in Fig. 14 where it is fitted with the logistic curve given by (11) and by arctan model given by (12). If we compare these two fits it is clear that both models fit the curve reasonably, however the first model describes the behavior better, especially for lower voltages. All other fits are therefore made using the logistic model. From this graph it is obvious that the threshold voltage for this module is 2 V. After reaching this voltage the polarization state changes rapidly.

Figures 15 and 16 show that the theoretical model agrees reasonably with the measured data. With increasing voltage, the output polarization state goes back to the input state and the LC device acts as identity operator. We can also notice that when threshold voltage is achieved the polarization change becomes more rapid. If voltage is not applied or is very low, the input polarization state changes to an elliptical polarization. When horizontal or vertical state is on input, the curve of the LC module crosses the equator on the Poincaré sphere (Fig. 15, parts H and V). It means that we can achieve another linear polarization by applying a certain voltage. This state is close to the perpendicular state to the input one. For H state on input the overlap of output state with V state is

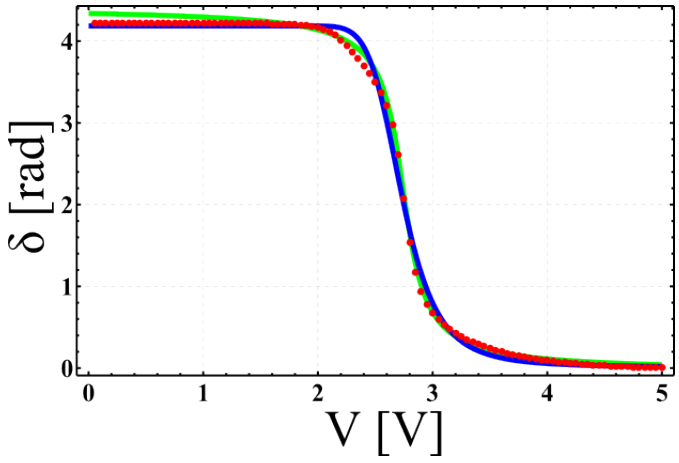

Figure 14: Dependence of retardance on voltage for RS module. Blue curve - fit to logistic model, green curve - fit to arctan model. Error bars are smaller than markers.

Input	DOP_{MIN}	DOP_{MAX}
H	0.982	1.005
V	0.968	1.013
D	0.96	0.99
A	0.980	0.999
R	0.95	0.98
L	0.95	1.00

Table 3: DOP maxima and minima for each input state for *RS 5080PHR 215-6442* module.

0.981 when 2.50 volts are applied to the module. The overlap of transformed V state with H state is 0.991. The analogous behavior appears when the input state is A (Figure 16, picture A). The curve crosses the equator almost exactly at D state with overlap 0.997. In Fig. 15, picture D, where the D state is at the input we can notice that the measured data almost touch the equator very close to A state with overlap 0.995 with A. The measured states and the corresponding voltages with calculated overlaps with states perpendicular to input state are in Tab. 4. Calculated values of parameters are: $a = 13.8$, $b = 3.3$, $c = -88.7$, $d = -0.1$, $e = -2.4$ and $f = 0$. Value of angle $\varphi = 4.9$ rad $\approx 281°$ and $\xi = 3.9$ rad $\approx 223°$. Statistical uncertainty of reconstructed Stokes parameters is in order of 10^{-3} but the real uncertainty is probably slightly higher due to another factors that impact the measurement.

Input $\|\psi\rangle$	Voltage [V]	Output $\|\phi\rangle$	DOP	$\|\langle\psi^{\perp}\|\phi\rangle\|^2$
H	2.50	$\begin{bmatrix} 1 \\ -0.962 \\ -0.105 \\ -0.22 \end{bmatrix}$	0.993	0.981
V	2.50	$\begin{bmatrix} 1 \\ 0.983 \\ 0.117 \\ 0.097 \end{bmatrix}$	0.995	0.991
D	2.45	$\begin{bmatrix} 1 \\ 0.021 \\ -0.991 \\ -0.058 \end{bmatrix}$	0.993	0.995
A	2.45	$\begin{bmatrix} 1 \\ 0.000 \\ 0.995 \\ -0.018 \end{bmatrix}$	0.995	0.997
R	2.65	$\begin{bmatrix} 1 \\ 0.040 \\ -0.021 \\ 0.953 \end{bmatrix}$	0.954	0.024
L	2.60	$\begin{bmatrix} 1 \\ -0.052 \\ 0.018 \\ -0.973 \end{bmatrix}$	0.974	0.014

Table 4: Polarization state trnsformations for RS module and the voltage applied of about 2.5 V and their overlaps with input state and state perpendicular to input state.

Temperature stability

Although liquid crystal displays are constructed to work in a wide range of temperature some structural changes may occur due to properties of liquid crystals. This measurement probes the affect of temperature changes on the performance of the module. To evaluate the effect of the presence of liquid crystal in the setup I have performed two similar mea-

surements, one with the liquid crystal in setup and one without it. For both configurations I have measured the same polarization state and temperature of the module 1000 times during 90 hours interval. The temperature changes were caused by temperature changes in laboratory. In the part of the experiment with the LC module there was fixed voltage of 2.5 V applied to the module. The results of each experiments, I have divided by temperature into 3 groups and plotted these subsets on Poincaré sphere in Fig. 17. I have calculated the covariance matrices for these measurements and their eigenvalues. They are shown in Tab. 5. I have also calculated the covariance matrix and its eigenvalues for each temperature interval in both measurements. Eigenvalues represent main variances. This is in tables 6 and 7. In Figs. 18 and 19,there are plotted measured states in plane S_1S_2 . I have calculated the average values for each temperature interval as well. Measured and calculated values show that if LC module is not in setup it is reasonably stable and measured polarization state does not depend on the temperature. On the other hand, if there is the LC module present in the setup, the variance of the measured state increase 10 times. If we compare positions of mean values for these measurements, see Tabs. 6 and 7, we can see that in setup without the LC module, the average value differs very slightly for all three temperature intervals and mean values do not "move"in one direction. However, if LC module is present in the setup, mean values do move in one direction for different temperature intervals, see Fig. 19. This shows that the retardation δ slightly decreases with growing temperature.

	Covariance matrix	Eigenvalues
without	$\begin{pmatrix} 9\cdot10^{-6} & -2\cdot10^{-6} & -1\cdot10^{-6} \\ -2\cdot10^{-6} & 6\cdot10^{-5} & -1\cdot10^{-6} \\ -1\cdot10^{-6} & -1\cdot10^{-6} & 7\cdot10^{-5} \end{pmatrix}$	$\begin{pmatrix} 7\cdot10^{-5} \\ 6\cdot10^{-5} \\ 9\cdot10^{-6} \end{pmatrix}$
with	$\begin{pmatrix} 2\cdot10^{-4} & 4\cdot10^{-6} & 3\cdot10^{-6} \\ 4\cdot10^{-6} & 7\cdot10^{-4} & 8\cdot10^{-6} \\ 3\cdot10^{-6} & 8\cdot10^{-6} & 8\cdot10^{-4} \end{pmatrix}$	$\begin{pmatrix} 8\cdot10^{-4} \\ 7\cdot10^{-4} \\ 2\cdot10^{-4} \end{pmatrix}$

Table 5: Comparsion of covariance matrices for setup with LC module and without it and their eigenvalues.

Temp. interval	Covariance matrix	Eigenvalues	$\bar{S_1}$	$\bar{S_2}$
[28.4; 29.0) °C	$\begin{pmatrix} 2\cdot10^{-6} & -5\cdot10^{-7} & 1\cdot10^{-6} \\ -5\cdot10^{-7} & 3\cdot10^{-5} & -5\cdot10^{-7} \\ 1\cdot10^{-6} & -6\cdot10^{-7} & 3\cdot10^{-5} \end{pmatrix}$	$\begin{pmatrix} 3\cdot10^{-5} \\ 3\cdot10^{-5} \\ 2\cdot10^{-6} \end{pmatrix}$	0.991	−0.026
[29.0; 29.6) °C	$\begin{pmatrix} 5\cdot10^{-5} & -2\cdot10^{-6} & -2\cdot10^{-6} \\ 2\cdot10^{-6} & 6\cdot10^{-5} & -5\cdot10^{-6} \\ -2\cdot10^{-6} & -5\cdot10^{-6} & 8\cdot10^{-5} \end{pmatrix}$	$\begin{pmatrix} 8\cdot10^{-5} \\ 6\cdot10^{-6} \\ 2\cdot10^{-5} \end{pmatrix}$	0.990	−0.026
[29.6; 30.5) °C	$\begin{pmatrix} 7\cdot10^{-6} & -2\cdot10^{-6} & -8\cdot10^{-7} \\ -2\cdot10^{-6} & 6\cdot10^{-5} & 7\cdot10^{-7} \\ -8\cdot10^{-7} & 7\cdot10^{-7} & 8\cdot10^{-5} \end{pmatrix}$	$\begin{pmatrix} 8\cdot10^{-5} \\ 7\cdot10^{-5} \\ 7\cdot10^{-6} \end{pmatrix}$	0.991	−0.025

Table 6: Covariance matrices of reconstructed states in three temperature intervals, their eigenvalues and mean values of Stokes parameters S_1 and S_2 for setup without LC module.

Temp. interval	Covariance matrix	Eigenvalues	$\bar{S_1}$	$\bar{S_2}$
[23.5; 24.1) °C	$\begin{pmatrix} 2\cdot10^{-4} & 2\cdot10^{-6} & -1\cdot10^{-5} \\ 2\cdot10^{-6} & 6\cdot10^{-4} & 3\cdot10^{-5} \\ -1\cdot10^{-5} & 3\cdot10^{-5} & 7\cdot10^{-4} \end{pmatrix}$	$\begin{pmatrix} 7\cdot10^{-4} \\ 6\cdot10^{-4} \\ 2\cdot10^{-4} \end{pmatrix}$	−0.869	−0.482
[24.1; 24.9) °C	$\begin{pmatrix} 2\cdot10^{-4} & 1\cdot10^{-5} & 6\cdot10^{-6} \\ 1\cdot10^{-5} & 7\cdot10^{-4} & 5\cdot10^{-5} \\ 6\cdot10^{-6} & 5\cdot10^{-5} & 8\cdot10^{-4} \end{pmatrix}$	$\begin{pmatrix} 8\cdot10^{-4} \\ 7\cdot10^{-4} \\ 3\cdot10^{-4} \end{pmatrix}$	−0.864	−0.485
[24.9; 25.5) °C	$\begin{pmatrix} 2\cdot10^{-4} & 5\cdot10^{-5} & 1\cdot10^{-5} \\ 5\cdot10^{-5} & 9\cdot10^{-4} & 1\cdot10^{-4} \\ 1\cdot10^{-5} & 1\cdot10^{-4} & 1\cdot10^{-3} \end{pmatrix}$	$\begin{pmatrix} 2\cdot10^{-3} \\ 9\cdot10^{-4} \\ 2\cdot10^{-4} \end{pmatrix}$	−0.862	−0.487

Table 7: Covariance matrices of states in temperature intervals, their eigenvalues and mean values os Stokes parameters S_1 and S_2 for setup with LC module RS 5080PHR 215-6442.

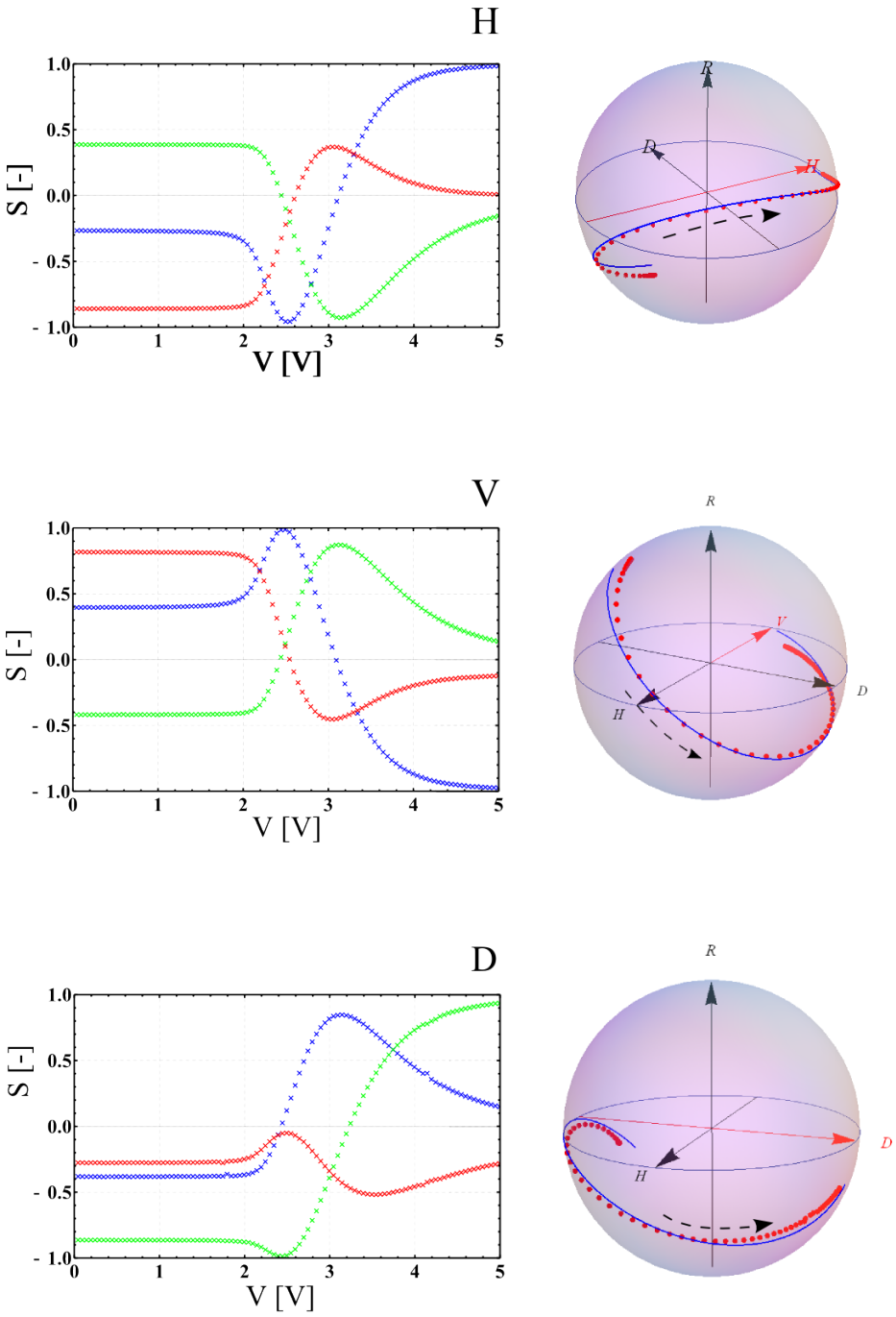

Figure 15: Transformation of polarization state by RS module while changing applied voltage and H, V and D state on input. On the left: graphs of Stokes parameters S_1 - blue, S_2 - green, S_3 - red. On the right: Poincaré sphere: measured states - red dots, fit - blue line. The dashed arrow represents direction of voltage growth. Error bars are smaller than markers.

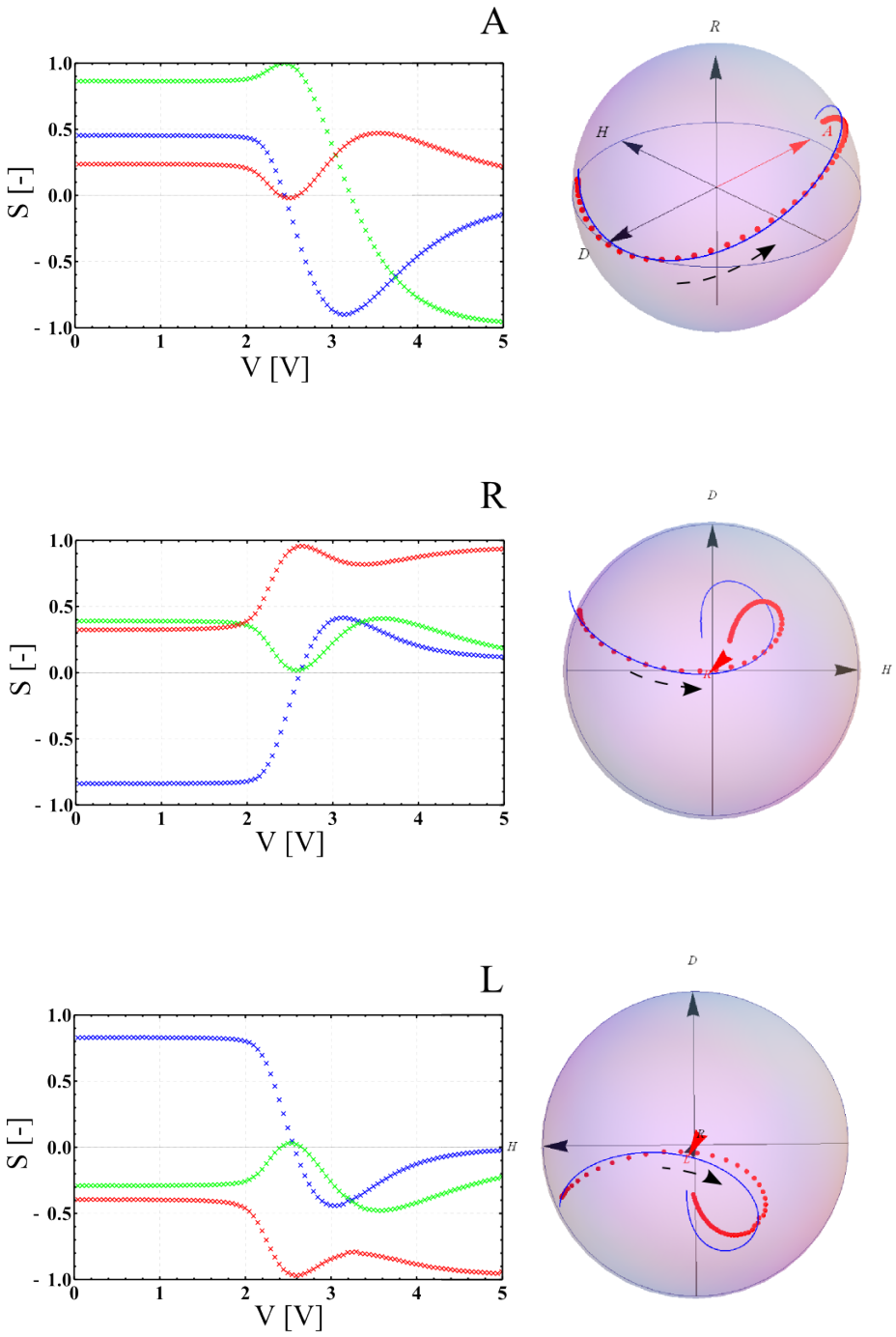

Figure 16: Transformation of polarization state by RS module while changing applied voltage and A, R and L state on input. On the left: graphs of Stokes parameters S_1 - blue, S_2 - green, S_3 - red. On the right: Poincaré sphere: measured states - red dots, fit - blue line. The dashed arrow represents direction of voltage growth. Error bars are smaller than markers.

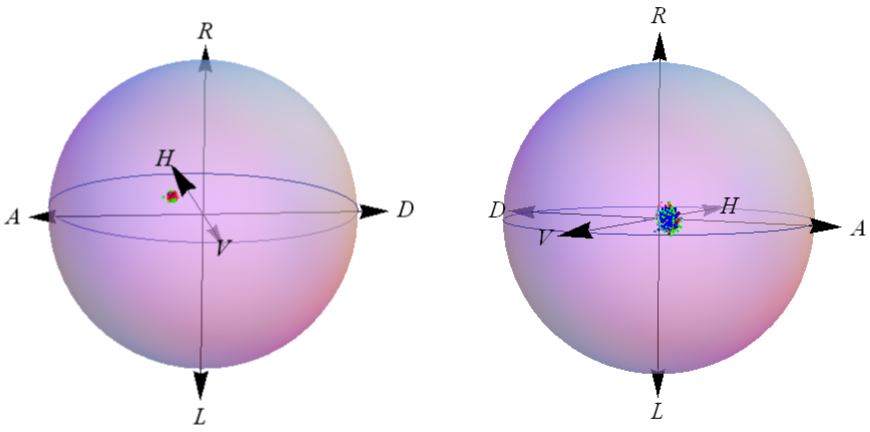

Figure 17: Measured states on Poincaré sphere for various temperatures. Left panel: the configuration without LC module, right panel configuration with the RS 5080PHR 215-6442 module with applied voltage 2.5 V.

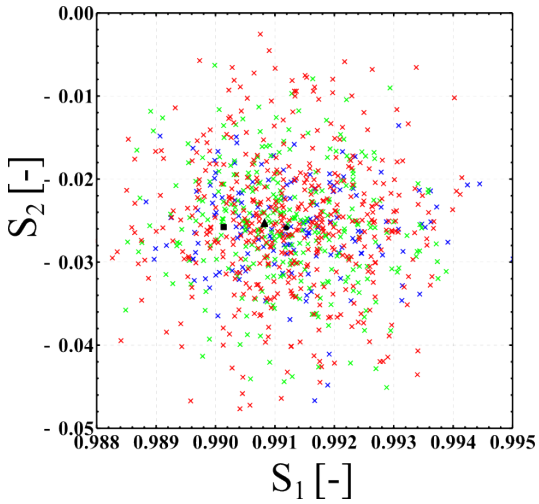

Figure 18: Measured states and their averages (black markers) in tangential plane S_1S_2 for setup without LC module. Blue dots and circle - temperature interval [28.4; 29.0) °C, green dots and square - temperature interval [29.0; 29.6) °C, red dots and triangle - temperature interval [29.6; 30.5) °C.

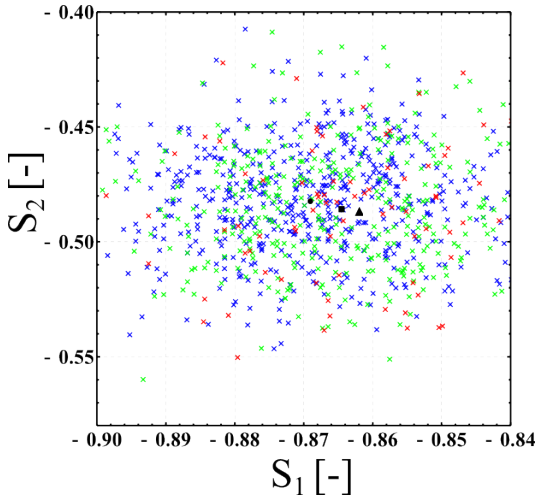

Figure 19: Measured states and their averages (black markers) in tangential plane S_1S_2 for setup with LC module with 2.5 V voltage applied. Blue dots and circle - temperature interval [23.5; 24.1) °C , green dots and square - temperature interval [24.1; 24.9) °C, red dots and triangle - temperature interval [24.9; 25.5) °C.

4.2 Segment module *OCZ 2027*

To study effects of this module on polarization state I have worked with the largest segment (no. 18) present in the module, see Fig. 10. The measurement was the same as I have done with the RS module. Figs. 21 and 22 show results of the measurement of polarization state change. From these images it is clear that different technology was used in this module compared to technology used in the RS module. The trajectory of the polarization state on the Poincaré sphere in this case is not as long as in the case of RS display, but it shows that polarization state does not change until threshold voltage of about 2 V is reached. Then the polarization state changes rapidly. In Fig. 20 there are plotted calculated values of retardance δ in dependence on voltage and fit on logistic curve and arctan model. It is clear that the logistic model fits the process much better. Calculated parameters for logistic model are: $a = 6.72$,$b = 11.49$, $c = 46.84$, $d = 0.139$, $e = -2$, $f = 0$, $\varphi = 4.34$ rad $\approx 249°$, $\xi = 0.06$ rad $\approx 3°$. Table 8 shows maxima and minima of DOP achieved for each input polarization state.

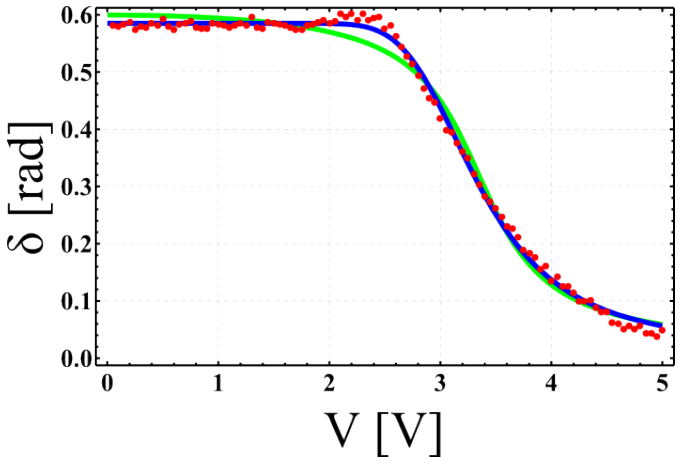

Figure 20: Dependence of retardance on voltage for OCZ 2027 module. Blue curve - fit to logistic model, green curve - fit to arctan model. Error bars are smaller than markers.

Measured data show fluctuation even though the statistical uncertainty is in order of 10^{-3}. This fluctuation might be caused by improper driving frequency used during measurement. This happened because the manufacturer did not provide us with this information before the measurement. For driving was used standard frequency 90 Hz. Designed frequency for this crystal however is 64 Hz. I suppose, that the real value of uncertainty is in order 10^{-3} or even higher. Table 8 shows minima and maxima of DOP for this display. These values are very similar to the values achieved with RS module.

Input	DOP_{MIN}	DOP_{MAX}
H	0.92	1.03
V	0.99	1.04
D	0.95	1.00
A	0.94	1.04
R	0.95	1.01
L	0.89	1.03

Table 8: DOP maxima and minima for each input state. OCZ 2027 module.

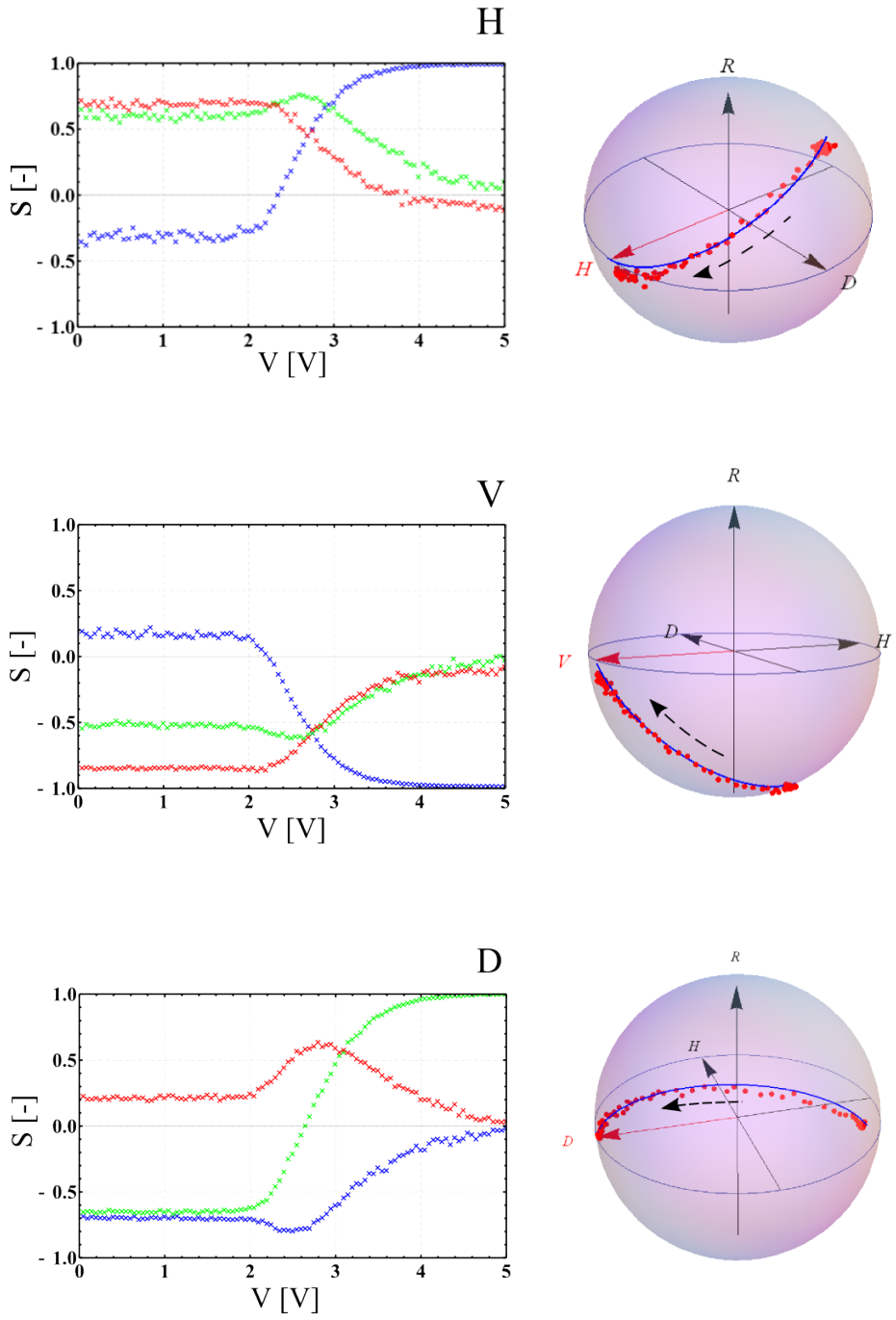

Figure 21: Transformation of polarization state by OCZ 2027 module while changing applied voltage and H, V and D states on input. On the left: graphs of stokes parameters S_1 - blue, S_2 - green, S_3 - red. On the right: Poincaré spheres: measured states - red dots, fit - blue line. The dashed arrow represents direction of voltage growth. Error bars are smaller than markers.

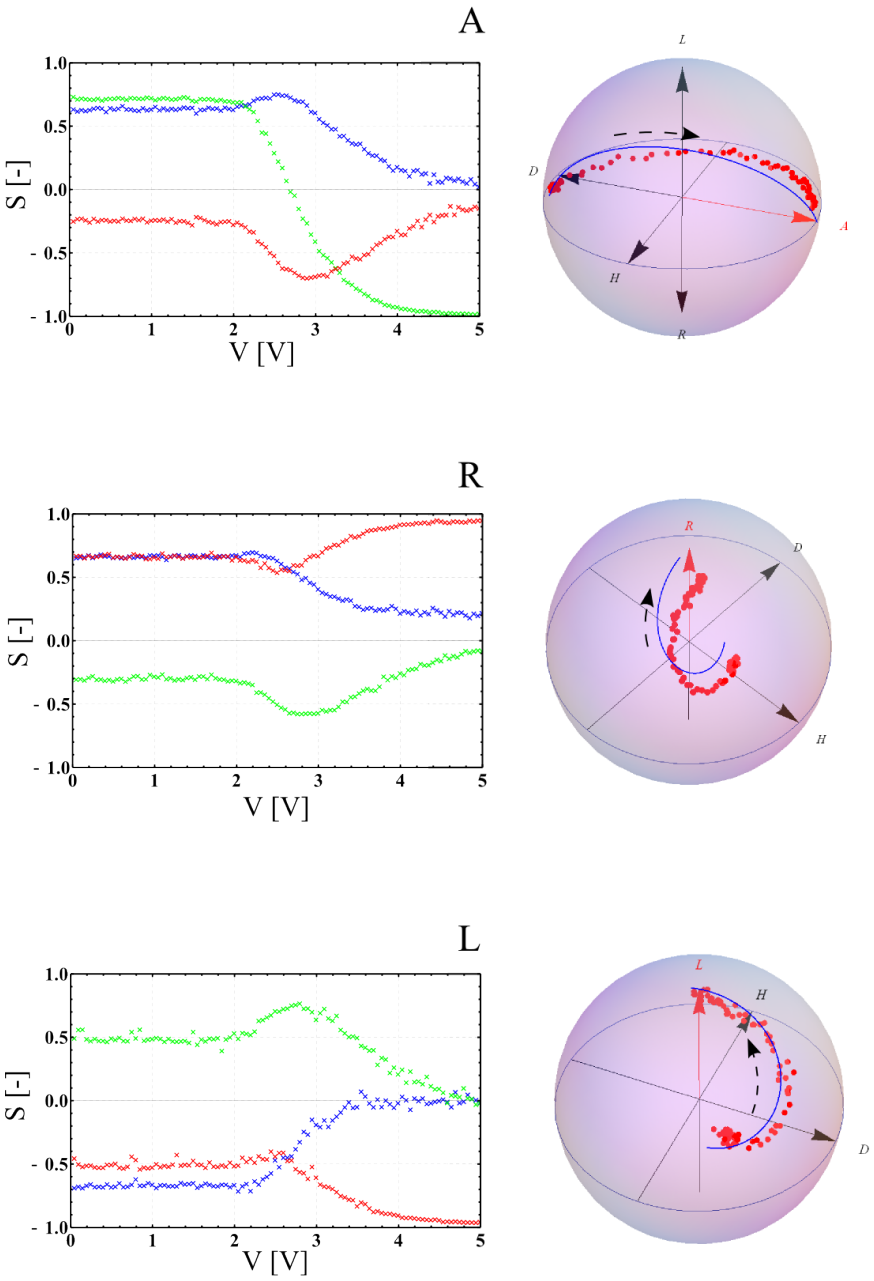

Figure 22: Transformation of polarization state by OCZ 2027 module while changing applied voltage and A, R and L state on input. On the left: graph of stokes parameters S_1 - blue, S_2 - green, S_3 - red. On the right: Poincaré sphere: measured states - red dots, fit - blue line. The dashed arrow represents direction of voltage growth. Error bars are smaller than markers.

"Gray level"	Output state	DOP	"Contrast"	Output state	DOP
0	$\begin{pmatrix} 1 \\ \text{-}0.070 \\ 0.549 \\ -0.747 \end{pmatrix}$	0.929	0	$\begin{pmatrix} 1 \\ \text{-}0.129 \\ 0.503 \\ -0.773 \end{pmatrix}$	0.931
1	$\begin{pmatrix} 1 \\ 0.059 \\ 0.562 \\ -0.714 \end{pmatrix}$	0.911	100	$\begin{pmatrix} 1 \\ 0.098 \\ 0.503 \\ -0.767 \end{pmatrix}$	0.922
2	$\begin{pmatrix} 1 \\ 0.506 \\ 0.209 \\ -0.680 \end{pmatrix}$	0.874	150	$\begin{pmatrix} 1 \\ 0.277 \\ 0.258 \\ -0.728 \end{pmatrix}$	0.821
3	$\begin{pmatrix} 1 \\ 0.601 \\ 0.163 \\ -0.638 \end{pmatrix}$	0.892	200	$\begin{pmatrix} 1 \\ 0.532 \\ 0.096 \\ -0.694 \end{pmatrix}$	0.881

Table 9: Transformed H state after propagation through DOG XL module with various values of "Gray level"and "Contrast "parameters.

4.3 Pixel modules

I have examined the transformation of H state by DOG XL 160 module by changing orientation of liquid crystals using controllable parameters (see Tab. 2). First, I have been changing "Gray level". I also did the same measurement also for "Contrast"change. The results of these measurement are shown in Tab. 9.

We can see that maximum achieved DOP in both measurements is ≈ 0.93. This is in perfect correspondence with the fill factor. This happens because a part of the light always goes through an area that is not influenced by applied voltage and so the light in this area feels different phase retardation then in areas affected by voltage. This causes depolarization of output state. The maximum achieved degree of polarization is probably not high enough to be used in polarization state preparation or filtering.

The similar measurement will be done also for pixel module OCZ 2001. This module has fill factor 0.88, lower than the DOG XL module, but it offers continuous voltage tuning. I expect the output degree of polarization to be around 0.88. This is probably too low for

use in polarization state preparation, measurement or filtering. However, it can be used as a variable depolarization channel.

5 Conclusion

In this Thesis, I have briefly described the basic principles of liquid crystal displays and their possible use for scientific purposes. The Mueller-Stokes formalism was used to determine the effect of liquid crystal on the polarization state of light and a set of measurements was performed to validate this theory and to probe other properties of liquid crystals. I have used various liquid crystal modules that are based on commercially available LC displays from which I have removed all polarization and protective layers.

I have focused on the transformation of the polarization state of light by liquid crystal. I have performed measurements on three different types of liquid crystal modules: two segment modules and one pixel module. First experiment I did with a simple segment module from RS company. This module uses basic TN technology and segments have shape like we know from digital displays, see Fig. 9. Measurements of output polarization state with different voltage applied to the module show that we can achieve various polarization states with the degree of polarization about 0.99 (see Tab. 3). Measurements also revealed that if voltage around 2.5 V is applied to the module with linearly polarized input light, we achieve almost perpendicular states with overlap 0.98 and higher. With this display I have also performed the temperature stability test that shows that there is a slight temperature dependence and the retardance δ slightly decreases with growing temperature. A more important discovery that brought this measurement is that the presence of liquid crystal in the setup increases the variance approximately 10 times. Technology used in this module seems to be the most suitable for purposes of Quantum Optics Laboratory Olomouc.

The second tested module was made by OCZ Vrchlabí type 2027 company and was sent to us as a sample. Its scheme is in Fig. 10. This module uses technology TN270. The experiments revealed shorter trajectory of the polarization state transformation, than in case of RS module, and it does not cross the equator or poles of the Poincaré sphere. It means that the maximum retardation is significantly lower and we are not able to get any other significant polarization state at the output as we could with the RS module. This technology therefore does not seem to be suitable for our purposes.

Last tested module was the pixel module DOG XL160. This display uses the STN technology and is operated via internal chip that allows us to control voltage applied to each segment but only in discrete steps. Controllable parameters are mentioned in Tab. 2. The fill factor of this display is 0.93. The results of my experiments show that maximal achieved degree of polarization was 0.93 or lower. It might be possible to use such devices as depolarization channel. Similar behavior is expected from the OCZ 2001 module which offers continuous voltage driving but its fill factor is lower. The potential use of this module

is therefore the same as of the DOG XL module.

The initial idea to start working with liquid crystals was to control the polarization state of two or more close parallel collimated laser beams from calcite splitters. The distance between two such beams is typically 4 or 6 mm. Tested modules, however do not have such option so we have decided to contact companies engaged in manufacturing LC modules: ArcOptix, Bolder Vision Optik, Meadowlark Optics, and OCZ Vrchlabí. Last mentioned company sent us few samples of their technology, one of this samples, the OCZ 2027, was put under test in this Thesis. The result of collaboration with this company is also a drawing of LC module suitable for purposes of Quantum Optics Laboratory Olomouc based on my sketch, see Fig. 23. The communication with Bolder Vision Optik resulted in sending a price quotation of such custom module. The average price of a custom device is about $1700 per module.

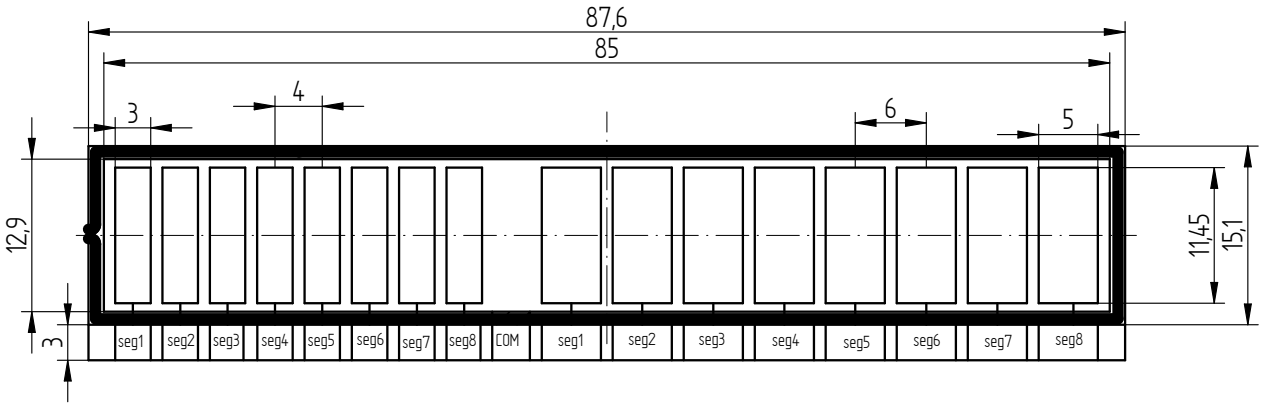

Figure 23: Sketch of future custom LC module made in collaboration with OCZ Vrchlabí company suitable for controlling up to eight parallel laser beams with separation 4 or 6 mm.

References

[1] H. Kawamoto, *The history of liquid-crystal displays*, Proceedings of the IEEE **90**, 460 (2002).

[2] R. H. Chen, Liquid crystal displays: fundamental physics and technology, (Wiley, Hoboken, N.J., 2011).

[3] O. Aharon and I. Abdulhalim, *Liquid crystal Lyot tunable filter with extended free spectral range*, Opt. Express **17**, 11426 (2009).

[4] K. Hirabayashi, *Electrically controllable liquid crystal rotatable wave plate with variable phase retardation*, Appl. Opt. **44**, 3552 (2005).

[5] J. M. Bueno, *Polarimetry using liquid-crystal variable retarders: theory and calibration*, J.Opt. A: Appl. Opt. **2**, 216 (2000).

[6] Z. Zhuang, S.-W. Suh and J. S. Patel, *Polarization controller using nematic liquid crystals*, Opt. Lett. **24**, 694 (1999).

[7] I.-C. Khoo and S.-T. Wu, Optics and nonlinear optics of liquid crystals, (World Scientific Publishing, Singapore, 1993).

[8] B. Saleh and M. Teich, Fundamentals of Photonics, (Wiley, Hoboken, N.J., 2007).

[9] R. G. Driggers, Encyclopedia of optical engineering, Volume 3, pp. 2169- 2175 (CRC Press, Cambridge, 2003).

[10] P. Hey and C. Gu, Optics of liquid crystal displays, (Wiley, Hoboken, N.J., 2010).

[11] J. Hoogboom, T. Rasing, A. E. Rowan, and R. J. M. Nolte, *LCD alignment layers. Controlling nematic domain properties*, J. Mater. Chem. **16**, 1305 (2006).

[12] K. Takatoh, M. Hasegawa, M. Koden, N. Itoh, R. Hasegawa and M. Sakamoto, Alignment technologies and applications of liquid crystal devices, (Taylor & Francis, London, 2005).

[13] V. G. Chigrinov, V. M. Kozenkov and H.-S. Kwok, Photoalignment of liquid crystalline materials: physics and applications, (Wiley, Chichester, West Sussex, 2008).

[14] S. H. Perlmutter, D. Doroski and G. Moddel, *Degradation of liquid crystal device performance due to selective adsorption of ions*, Appl. Phys. Lett. **69**, 1182 (1996).

[15] A. Mochizuki, K. Motoyoshi and S. Kobayashi, *A ferroelectric layer in a cell containing a polar molecular mixture in nematic and isotropic phases*, J. Mater. Chem.**16**, 1305 (2006).

[16] D. Lundström and J. Yilbar, *Liquid crystal materials* [online]. [cit. 2014-05-06]. Available from `http://www.kth.se/fakulteter/_TFY/kmf/lcd/lcd~1.htm`.

[17] S. Huard, Polarization of light, (Willey, Cambridge, 2003).

[18] ArcOptix Variable phase retarder datasheet, [online].[cit. 2014-05-06]. Available from `http://www.arcoptix.com/ARCoptix%20Phase%20Retarder.pdf`.

[19] S. T. Tang and H. S. Kwok, *Mueller calculus and perfect polarization conversion modes in liquid crystal displays*, J. Appl. Phys. **89**, 5288 (2001).

[20] A. Vargas, R. Donso, M. Ramírez, J. Carrión, M. del Mar Sánchez-López and I. Moreno, *Liquid crystal retarder spectral retardance characterization based on a cauchy dispersion relation and a voltage transfer function*, Opt. Rev. **20**, 378 (2013).

[21] 780-HP Nufern Single mode fiber, [online]. [cit. 2014-05-06]. Available from `http://www.nufern.com/pam/optical_fibers/883/780-HP/`.

[22] Datasheet Tektronix AFG3252, [online]. [cit. 2014-05-08]. Available from `http://www.tek.com/sites/tek.com/files/media/media/resources/AFG3000_Series_Arbitrary-Function_Generators_Datasheet_76W-18656-5.pdf`.

[23] Electronic display datasheet, [online]. [cit. 2014-06-05]. Available from `http://docs-europe.electrocomponents.com/webdocs/001b/0900766b8001b54d.pdf`.

[24] Library dogm128, [online]. [cit. 2014-05-06]. Available from `http://code.google.com/p/dogm128/`.

[25] DOG XL graphics series datasheet, [online]. [cit. 2014-05-07]. Available from `http://www.lcd-module.com/eng/pdf/grafik/dogxl160-7e.pdf`.